(pentyloxy)phenyl]acetylene, 129921-33-1; 1,2-bis[3-fluoro-4-(hexyloxy)phenyl]acetylene, 129921-34-2; 1,2-bis[3-fluoro-4-(heptyloxy)phenyl]acetylene, 129921-35-3; 1,2-bis[3-fluoro-4-(octyloxy)phenyl]acetylene, 129921-36-4; 1,2-bis[3-fluoro-4-(nonyloxy)phenyl]acetylene, 129921-37-5; 1,2-bis[3-fluoro-4-(decyloxy)phenyl]acetylene, 129921-38-6; 1,2-bis[3-fluoro-4-(decyloxy)phenyl]acetylene, 129921-39-7; 1,2-bis[3-fluoro-4-(dodecyloxy)phenyl]acetylene, 129921-40-0; 1-[3-fluoro-4-(pentyloxy)phenyl]-2-[4-(pentyloxy)phenyl]acetylene, 129921-41-1; 1-[3-fluoro-4-(hexyloxy)phenyl]-2-[4-(hexyloxy)phenyl]acetylene, 129921-42-2; 1-[3-fluoro-4-(heptyloxy)phenyl]-2-[4-(heptyloxy)phenyl]acetylene, 129921-43-3; 1-[3-fluoro-4-(octyloxy)phenyl]-2-[4-(octyloxy)phenyl]acetylene, 129921-44-4; 1-[3-fluoro-4-(nonyloxy)phenyl]-2-[4-(nonyloxy)phenyl]acetylene, 129921-45-5; 1-[3-fluoro-4-(decyloxy)phenyl]-2-[4-(decyloxy)phenyl]acetylene, 129942-72-9; 1-[3-fluoro-4-(undecyloxy)phenyl]-2-[4-(undecyloxy)phenyl]acetylene, 129942-73-0; 1-[3-fluoro-4-(dodecyloxy)phenyl]-2-[4-(dodecyloxy)phenyl]acetylene, 129942-74-1.

Characterization of the $Bi_{1.6}Pb_{0.4}Sr_2Ca_2Cu_3O_y$ Superconductor by X-ray Diffraction, Low-Field Microwave Absorption, and Electron Spin Resonance

Stephane Cuvier, Micky Puri,* John Bear, and Larry Kevan*

Department of Chemistry and the Texas Center for Superconductivity, University of Houston, Houston, Texas 77204-5641

Received May 30, 1990. Revised Manuscript Received September 19, 1990

X-ray diffraction (XRD) and low-field microwave absorption (LFMA) have been measured for a series of $Bi_{1.6}Ph_{0.4}Sr_2Ca_2Cu_3O_y$ superconducting samples prepared at different sintering temperatures that display zero resistance between 50 and 98 K. Multiphase formation is observed in all samples. XRD results suggest that the fraction of the high-transition temperature (T_c) phase denoted as 2223 grows with increasing sintering time and temperature compared to the low-T_c phase denoted as 2212, although the 2212 phase always predominates. Simultaneously, several impurity phases also increase. The 2223 phase and 2210 phase seem to be formed by the disproportionation of the 2212 phase. The incorporation of Pb in the lattice accelerates this disproportionation process. LFMA signals reveal the presence of two superconducting phases with T_c close to 75 and 115 K. The intensity of the microwave absorption due to the low T_c phase is 3–6 times higher than that of the high T_c phase. This suggests that between the two transition temperatures, the magnetic shielding of the high T_c phase is weakened by penetration of the magnetic flux in the bulk material through the low T_c phase, when the latter becomes nonsuperconducting above its transition temperature. No electron spin resonance signal has been detected for this superconducting system above or below T_c, which indicates the lack of paramagnetic impurity phases.

Introduction

It is generally accepted that the two high-temperature superconducting phases in the BiSrCaCuO system have nominal compositions of $Bi_2Sr_2CaCu_2O_y$ (2212) with T_c near 80 K and $Bi_2Sr_2Ca_2Cu_3O_y$ (2223) with T_c near 110 K.[1-5] The $Bi_2Sr_2CuO_y$ phase (2201) is a low-temperature superconductor with a $T_c \sim 10$ K. The 2212 phase formation is the most facile, and hence it always is the dominant species. It is more difficult to prepare the 2201 and 2223 phases. It has been shown by Cava et al.[6] that Pb substitution for Bi promotes the formation of the 2223 phase when the correct stoichiometric amounts of starting materials are used. A 10–30 mol % Pb substitution for Bi is reported to be the optimum ratio for 2223 phase formation.[7-11] Furthermore, lead substitution also appears to affect the speed of reaction so that similar material can be produced in a shorter time.[11,12]

Other methods reported to accelerate the formation of the 2223 phase are sintering under reduced oxygen partial pressure,[9] modification of starting composition,[9,13] careful control of sintering temperature,[7,8,14,15] antimony[16] and/or vanadium[17] substitution for bismuth, and partial replacement of oxygen by fluorine.[18] A reduction in oxygen content to enhance T_c of the 2212 phase has been accomplished by quenching,[19,20] argon, nitrogen, or hydrogen treatment, and thermal cycling.[15,21] Even without Pb substitution, a T_c above 95 K has been reported.[20,27]

* To whom correspondence should be addressed at the Department of Chemistry.

(1) Michel, C.; Hervieu, M.; Borel, M. M.; Grandin, A.; Deslandes, F.; Provost, J.; Raveau, B. *Z. Phys. B* **1987**, *68*, 421.
(2) Maeda, H.; Tanaka, Y.; Fukutomi, M.; Asano, T. *Jpn. J. Appl. Phys.* **1988**, *27*, 209.
(3) McGuire, T. R.; Shivashankav, S. A.; La Placa, S. J.; Chandrashekhar, G. V.; Boehme, R. F.; Shaw, T. M.; Yee, D. S.; Shafer, M. W.; Cuomo, J. J. *J. Appl. Phys.* **1988**, *64*, 5792.
(4) Dabrowski, B.; Richards, D. R.; Hinks, D. G.; Hannon, R. H.; Peng, W.; Lee, H.; Genis, A. P.; Melim, V. I.; Kimball, C. W. *Physica C* **1989**, *160*, 281.
(5) Torardi, C. C.; Subramanian, M. A.; Calabrese, J. C.; Gopalakrishnan, J.; McCarron, E. M.; Morrissey, K. J.; Askew, T. R.; Flippen, R. B.; Chowdry, U.; Sleight, A. W. *Phys. Rev. B* **1988**, *38*, 225.
(6) Cava, R. J.; Batlogg, B.; Sunshine, S. A.; Siegrist, T.; Fleming, R. M.; Babe, R.; Shneemeyer, L. F.; Murphy, D. W.; van Dover, R. B.; Gallagher, P. K.; Glarum, S. H.; Nakahara, S.; Farrow, R. C.; Krajewski, J. J.; Zahurak, S. M.; Waszcak, J. V.; Marshall, J. H.; Marsh, P.; Rupp Jr., L. W.; Peck, W. F.; Rietman, E. A. *Physica C* **1988**, *158*, 247.
(7) Oota, A.; Kirihigashi, A.; Sasaki, Y. Y.; Ohba, K. *Jpn. J. Appl. Phys.* **1988**, *27*, 2050.
(8) Koyama, S.; Endo, U.; Kawai, T. *Jpn. J. Appl. Phys.* **1988**, *27*, 1861.
(9) Endo, U.; Koyama, S.; Kawai, T. *Jpn. J. Appl. Phys.* **1989**, *28*, 190.
(10) Liu, H. K.; Dou, S. X.; Savvides, N.; Zhou, J. P.; Tan, M. X.; Bourdillon, A. J.; Kviz, M.; Sorrell, C. C. *Physica C* **1989**, *157*, 93.
(11) Flower, M. E.; Presland, M. R.; Gilberd, P.; Buckley, R. G. *Physica C* **1990**, *165*, 161.
(12) Mohan Ram, R. A.; Kobiela, P. S.; Kirk, W. P.; Clearfield, A. *J. Solid State Chem.* **1989**, *83*, 214.
(13) Sasakura, H.; Minamigawa, Nakahigachi, K.; Kogachi, M.; Nakanishi, S.; Fukuoka, N.; Yoshikawa, M.; Noguchi, S.; Okuda, K.; Yanase, A. *Jpn. J. Appl. Phys.* **1989**, *28*, 1163.

0897-4756/91/2803-0115$02.50/0

Though it is well established that the volume fraction of the 2223 phase can be substantially increased, the mechanism for this is not understood. Pb substitution for Bi is considered to increase the chemical stability of the 2223 phase,[22] while others consider that lead addition promotes the formation of a melt that is favorable for the growth of the high-T_c phase.[23] Higher concentrations of Ca_2CuO_3 impurity phases have been detected during the 2212 phase formation,[14] while Ca_2PbO_4 is considered to play a important role in the growth of the 2223 phase.[24] Tarascon et al. suggest that the 2223 phase forms from the 2212 phase through a nucleation process.[25] All these investigations suggest the desirability for additional research aimed at clarifying the actual role of lead in the formation of the 2223 phase in the presence of the 2212 phase.

In this paper, we present the results of the development of various phases grown from a matrix with the $Bi_{1.6}Pb_{0.4}Sr_2Ca_2Cu_3O_y$ stoichiometry. Our approach has been to carefully characterize polycrystalline multiphase samples to evaluate the possible mechanism for the formation of the 2223 phase from the 2212 phase. Characterization by X-ray diffraction, resistance, scanning electron microscopy, energy-dispersive microanalysis, low-field microwave absorption, and electron spin resonance (ESR) are carried out. Low-field microwave absorption (LFMA) has been shown to be an extremely sensitive diagnostic tool to study the local structure in such materials and to establish the critical superconducting temperature (T_c) accurately.[26-29] So far, only a few microwave absorption studies have been focused on the Bi–Sr–Ca–Cu–O and Bi–Pb–Sr–Ca–Cu–O systems. With the LFMA technique, it is possible to detect and compare the behavior of these two major superconducting phases.

The detection of the intense microwave absorption near zero field, with a long tail stretching toward higher fields by a conventional ESR spectrometer, is of considerable interest.[26-38] The response not only has been observed for the recently discovered copper oxide superconductors but has also been observed in superconducting granular aluminum films,[39] mercury,[40] and lead spheres.[41] Blazey et al. suggested that the absorption is a result of trapped magnetic flux in superconducting materials that show spin glass behavior.[42] However, the spin glass model based on the work of Stroud et al. fails to account for the observed nonlinear effects under field modulation.[43,44] It is generally agreed that the low-field response is related to intrinsic Josephson junctions in these materials. These occur where superconducting regions are separated by nonsuperconducting regions at grain boundaries or internal grain defects. LFMA has been attributed to the circulation of Josephson currents induced by the applied microwave energy.[45] Recently, Dulcic et al.[46] developed a line-shape model of the LFMA response based on the power absorbed in Josephson junctions in the surface of a superconductor; this model appears to satisfactorily explain the main experimental results.[47] The current LFMA investigations on a series of $Bi_{1.6}Pb_{0.4}Sr_2Ca_2Cu_3O_y$ samples are targeted toward the application of this unique response to multiphase granular superconductors.

Experimental Section

The samples were prepared by solid-state reaction from PbO, Bi_2O_3, $SrCO_3$, $CaCO_3$, and CuO. These oxides and carbonates were ground with a $Bi_{1.6}Pb_{0.4}Sr_2Ca_2Cu_3$ stoichiometry and heated at 1063 K for 20 h in air. The resulting material was reground, and pellets were pressed and heated at 1133, 1123, 1143, or 1153 K for 40 h. The samples were then reground, repelletized, and heated for an additional 40 h at each temperature. All the samples were allowed to cool in the furnace after it was turned off. This corresponds to cooling from ~1000 to ~900 K in about 2 h and from ~900 K to room temperature in about 6 h. Samples are named according to the sintering temperature in kelvin and the sintering time at this temperature in hours. For example, Pb/1133/40 has been calcined at 1063 K for 20 h and sintered at 1133 K for 40 h. A small piece of sample is cut from each pellet for a resistance measurement, and the rest of the sample is reground (particle size <25 μm) for microwave absorption experiments.

Powder X-ray diffraction (XRD) was performed on a D-5000 Siemens diffractometer, using Cu Kα radiation with nickel filters at 45 kV and 40 mA. The instrument was calibrated by using quartz as an external standard. In the 2–70° range of 2θ, a step size of 0.03° s^{-1} was used with 2-mm divergence and scatter slits and a 0.2-mm receiving slit. A computer program implementing the procedure of Appleman and Evans, developed by Garvey[48] is utilized for the least-squares unit cell refinements of the powder

(14) Sarkar, A. K.; Maartense, I.; Kumar, B.; Peterson, T. L. *Supercond. Sci. Technol.* **1990**, *3*, 199.
(15) Mohan Ram, R. A.; Clearfield, A.; Kobiela, P. S.; Kirk, W. P. *Physica C* **1990**, *166*, 125.
(16) Xu, Q.; Cheng, T.; Guang-Li, X.; Yang-Li, F. C.; Wang, H.; Mao, Z.; Peng, D.; Chen, Z.; Zhang, Y. *Physica C* **1990**, *168*, 489.
(17) Fung, P. C. W.; Lin, Z. C.; Liu, Z. M.; Xin, Y.; Sheng, Z. Z.; Chan, F. T.; Wong, K. W.; Xu, Y.; Ching, W. Y. *Solid State Commun.* **1990** *75*, 211.
(18) Gao, X.; Wu, X.; Yan, H.; Yin, Z.; Lin, C.; Fu, Y.; Xie, W. *Mod. Phys. Lett.* **1990**, *4*, 137.
(19) Xiaolin, H. W.; Shang, W. S.; Wang, Z.; Lu, Z.; Jiang, M. *Appl. Phys. Lett.* **1990**, *57*, 710.
(20) Kambe, S.; Matsuoka, T.; Takahasi, M.; Kawai, M.; Kawai, T. *Phys. Rev. B* **1990**, *42*, 2669.
(21) Sarkar, A. K.; Maartense, I. *Physica C* **1990**, *168*, 591.
(22) Ramesh, R.; Tenderco, van, G.; Thomas, G. G.; Luo, H. L. *Appl. Phys. Lett.* **1988**, *53*, 2220.
(23) Konstantinov, K.; Karbanov, S.; Souleva, A.; Kovacheva, D. *Supercond. Sci. Technol.* **1990**, *3*, 309.
(24) Tatsumisago, M.; Tsuboi, S.; Tohge, N.; Minami, T. *Appl. Phys. Lett.* **1990**, *57*, 195.
(25) Tarascon, J. M.; LePage, Y.; Greene, L. H.; Bagley, B. G.; Barboux, P.; Hwang, D. M.; Hull, G. W.; McKinnon, W. R.; Giroud, M. *Phys. Rev. B* **1988**, *38*, 2504.
(26) Pakulis, E. J.; Osada, T. *Phys. Rev. B* **1988**, *37*, 5790.
(27) Adrian, F. J.; Bohandy, J.; Kim, B. F.; Moorjani, K.; Wallace, J. S.; Shull, R. D.; Swartzendruber, L. J.; Bennett, L. H. *Physica C* **1988**, *156*, 184.
(28) Vier, D. C.; Oseroff, S. B.; Scilling, C. T.; Smyth, J. F.; Shultz, S.; Dauchaouch, Y.; Lee, B. W.; Maple, M. B. *Phys. Rev. B* **1987**, *36*, 8888.
(29) Kevan, L.; Bear, J.; Puri, M.; Yao, C. L. *Am. Chem. Soc., Symp. Ser.* **1988**, *58*, 1143.
(30) Tyagi, S.; Barsoum, M.; Rao, K. V.; Skumryev, V.; Yu, Z.; Costa, J. L. *Physica C* **1988**, *156*, 73.
(31) Owens, F. J.; Iqbal, Z. *Solid State Commun.* **1988**, *68*, 523.
(32) Bombik, A.; Korczak, S. Z.; Korczak, W.; Mazurek, P.; Pacyna, A. W.; Subotowicz, M.; Wysokinski, K. I. *Physica C* **1989**, *157*, 251.
(33) Dulcic, A.; Crepeau, R. H.; Freed, J. H. *Phys. Rev. B* **1989**, *39*, 4249.
(34) Calestani, G.; Rizzoli, C.; Andreetti, G. D.; Buluggiu, E.; Giori, D. C.; Valenti, A.; Vera, A.; Amoretti, G. *Physica C* **1989**, *158*, 217.
(35) Rakvin, B.; Pozek, M.; Paljevic, M.; Bricevic, N. *Solid State Commun.* **1989**, *70*, 729.
(36) Pozek, M.; Dulcic, A.; Rakvin, B. *Solid State Commun.* **1989**, *70*, 889.
(37) Marcon, R.; Fastampa, R.; Giura, M.; Matacotta, C. *Phys. Rev. B* **1989**, *39*, 2796.
(38) Pakulis, E. J.; Chandrashekhar, G. V. *Phys. Rev. B* **1989**, *39*, 808.
(39) Suss, J. T.; Berlinger, W.; Portis, A. M.; Müller, K. A. *Solid State Commun.* **1989**, *71*, 929.
(40) Rubins, R. S.; Black, T. D.; Jeong, D. Y. *Phys. Rev. B* **1989**, *40*, 2551.
(41) Rubins, R. S.; Hutton, S. L.; Drumheller, J. E. *Phys. Rev. B* **1989**, *39*, 4666.
(42) Blazey, K. W.; Müller, K. A.; Bednorz, J. G.; Berlinger, N.; Amoretti, G.; Buluggiu, E.; Vera, A.; Matacotta, F. C. *Phys. Rev. B* **1987**, *36*, 7241.
(43) Ebner, C.; Stroud, D. *Phys. Rev. B* **1985**, *31*, 165.
(44) Xia, T. K.; Stroud, D. *Phys. Rev. B* **1989**, *39*, 4792.
(45) Shrivastava, K. N. *J. Phys. C* **1987**, *20*, 789.
(46) Dulcic, A.; Rakvin, B.; Pozek, M. *Europhys. Lett.* **1989**, *10*, 593.
(47) Masiakowski, J.; Puri, M.; Cuvier, S.; Romanelli, M.; Schwartz, R. N.; Kimura, H.; Kevan, L. *Physica C* **1990**, *166*, 140.
(48) Garvey, R. G. Software product from Siemens based on the method of: Visser, J. W. *J. Appl. Cryst.* **1969**, *1*, 108.

Table I. Relative XRD Peak Intensities and Impurity Phases Detected for the $Bi_{1.6}Pb_{0.4}Sr_2Ca_2Cu_3O_y$ System under Various Sintering Conditions

	phase								
sample treatment	2223, 4.7°	2212, 5.7°	2223, 23.9°	2212, 27.5°	Ca_2PbO_4, 17.7°	Ca_2CuO_3, 36.8°	$Bi_2Sr_3O_z$, 16.7°	CaO_4, 64.6°	other phases
Pb/1123 K/40 h		100		100	5.0		4.0		$BiSr_3O_z$, $Bi_2Sr_3Cu_2O_z$
Pb/1123 K/80 h	17	100	3.8	100	5.0	4.6	3.3		$BiSr_3O_z$, $Bi_2Sr_3Cu_2O_z$ $Bi_{2.12}Sr_{1.87}Cu_{1.03}O_x$
Pb/1133 K/40 h	16	100	4.5	100	4.2		3.5		$BiSr_3O_z$, $Bi_2Sr_3Cu_2O_z$
Pb/1133 K/80 h	20	100	6.9	100	5.0	2.3	3.4	4.2	$BiSr_3O_z$, $Bi_2Sr_3Cu_2O_z$ $Bi_{2.12}Sr_{1.87}Cu_{1.03}O_x$
Pb/1143 K/40 h	21	100	5.7	100	4.2		4.1	3.3	$Bi_{2.12}Sr_{1.87}Cu_{1.03}O_y$, $Bi_2Sr_3Cu_2O_z$
Pb/1143 K/80 h	22	100	10.8	100		4.1	2.8	3.6	PbO_2, $Bi_2Sr_3Cu_2O_z$, $BiSr_3O_z$
Pb/1153 K/40 h	52	100	32	100		5.8	5.2		PbO_2,$BiSr_3O_z$,
Pb/1153 K/80 h	78	100	40	100			5.7		$Bi_{2.12}Sr_{1.87}Cu_{1.03}O_x$ PbO_2,$SrPbO_3$,Sr_2PbO_4,$BiSr_3O_z$, $Bi_2Sr_3Cu_2O_z$, $Bi_4Sr_8Cu_5O_z$

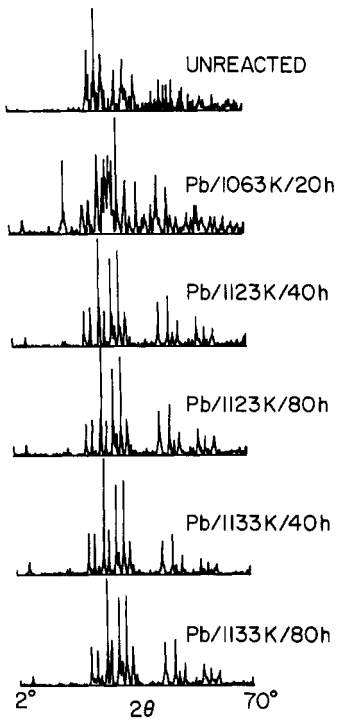

Figure 1. XRD for unreacted and $Bi_{1.6}Pb_{0.4}Sr_2Ca_2O_y$ samples Pb/1063/20, Pb/1123/40, Pb/1123/80, Pb/1113/40, and Pb/1113/80 as a function of sintering temperature and time in the 2θ range 2–70°.

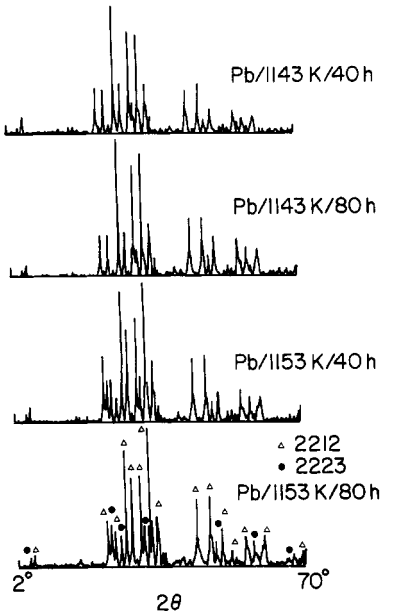

Figure 2. XRD for $Bi_{1.6}Pb_{0.4}Sr_2Ca_2O_y$ samples Pb/1143/40, Pb/1143/80, Pb/1153/80, Ph/1153/40, and Pb/1153/80 as a function of sintering temperature and time in the 2θ range 2–70°.

diffraction data.

Resistance measurements were performed using a standard four-probe method with a constant ac current of 130 μA at a frequency of 17 Hz. The voltage drop was detected by a lockin amplifier.

A Bruker ER 300 electron spin resonance (ESR) spectrometer equipped with an Oxford Instruments helium flow system was used to record low-field microwave absorption (LFMA) and ESR signals with a 10-G modulation amplitude and a microwave power of 2 mW. Each sample (5 mg) was placed in Suprasil quartz tubes that were evacuated and sealed. External coils were mounted on the poles of the magnet to compensate for the residual magnetic field and to enable sweeping from a negative magnetic field. The range −10 to 250 G through 0 G was scanned at each temperature after about 10 min was allowed for the temperature to equilibrate. It was found necessary to scan initially two or three times to get reproducible LFMA intensities. The temperature was increased in steps of 5 K from 4 K upward. The temperature at the sample position was monitored by an external thermocouple directly in contact with the sample tube in the microwave cavity.

A scanning electron microscope (SEM) from Cambridge Instruments (Model 250 MK3) was used to characterize the samples and examine crystallite formation as well as grain size distribution. Electron probe microanalysis of the sample was carried out on a 140-10 EDAX, energy-dispersive absorption of X-rays.

Results

XRD Analysis. The powder diffraction patterns for the unreacted, ground, stoichiometric material and after each heat treatment step are shown in Figures 1 and 2 in the 2θ range 2–70°. The heated samples show the dominant diffraction peaks that have been assigned to the 2212 phase (2θ = 5.7°, 23.2°, 27.5°) and to the 2223 phase (2θ = 4.7°, 23.9°, 28.8°, 33.8°) as well as peaks from PbO_2, Ca_2PbO_4, Ca_2CuO_3, CaO_4, $SrPbO_3$, Sr_2PbO_4, $BiSr_3O_z$, $Bi_2Sr_3Cu_2O_z$, and $Bi_{212}Sr_{187}Cu_{103}O_z$.[49-55]

(49) Hoongbao, L.; Xiaonong, Z.; Yaozu, C.; Guien, Z.; Ruan, Y.; Zhajia, C.; Yuheng, Z. *Physica C* **1988**, *156*, 804.
(50) Yang, C. Y.; Wen, J. G.; Yan, K. Y. F.; Fung, K. K. *Physica C* **1989**, *160*, 161.
(51) Onoda, M.; Yamato, A.; Muromachi, E. T.; Takekawa, S. *Jpn. J. Appl. Phys.* **1988**, *27*, 833.
(52) Cabrera, W. C.; Göpel, W. *Physica C* **1989**, *161*, 373.
(53) Pissas, M.; Niarchos, D. *Physica C* **1989**, *157*, 643.
(54) Ikeda, Y.; Ito, H.; Shimomura, S.; Oue, Y.; Inaba, K.; Hiro, Z.; Takano, M. *Physica C* **1989**, *159*, 93.
(55) Uzumaki, T.; Yamanaka, K.; Kamehara, N.; Niva, K. *Jpn. J. Appl. Phys.* **1989**, *28*, 75.
(56) Cuvier, S.; Puri, M.; Bear, J.; Kevan, L. *J. Phys. Chem.* **1990**, *94*, 6094.

Table II. Unit Cell Dimensions for the 2212 and 2223 Phase Determined as a Function of Sintering Time and Temperature (Standard Deviations in Parentheses)

sample treatment	unit cell data					
	2212			2223		
	a, Å	c, Å	ν, Å^3	a, Å	c, Å	ν, Å^3
Pb/1063 K/20 h	5.351 (1)	30.895 (4)	885			
Pb/1123 K/40 h	5.391 (2)	30.785 (2)	895	5.421 (3)	37.176 (4)	1093
Pb/1123 K/80 h	5.387 (4)	30.773 (3)	893	5.420 (3)	37.208 (2)	1093
Pb/1133 K/40 h	5.393 (1)	30.825 (2)	896	5.426 (1)	37.008 (2)	1090
Pb/1133 K/80 h	5.394 (2)	30.793 (1)	896	5.427 (2)	37.022 (3)	1090
Pb/1143 K/40 h	5.3900 (1)	30.780 (2)	894	5.421 (3)	37.047 (2)	1090
Pb/1143 K/80 h	5.386 (4)	30.743 (3)	892	5.420 (3)	37.176 (2)	1092
Pb/1153 K/40 h	5.383 (1)	30.733 (2)	891	5.422 (2)	37.160 (1)	1092
Pb/1153 K/80 h	5.395 (2)	30.714 (1)	894	5.431 (3)	37.081 (1)	1092

Since the starting composition for all the samples is $Bi_{1.6}Pb_{0.4}Sr_2Ca_2Cu_3O_7$, one would not expect only the 2212 phase ($T_c \sim 80$ K) or the 2223 phase ($T_c \sim 110$ K) unless all the Pb is incorporated in the Bi sites in the 2223 structure. The predominant phase in all our samples is the 2212 phase. The relative growth of the superconducting 2212 and 2223 phases can be compared from the intensities of the 4.7° peak assigned to the 2223 phase relative to the 5.7° peak assigned the 2212 phase. The intensity of the peak assigned to the 2223 phase is found to increase with increasing sintering time and temperature (Table I). A similar trend is also obtained on comparing the relative peak intensities at $2\theta = 23.9°$ (2223 phase) and at 27.5° (2212 phase). However since these two intensities are not well resolved, they do not agree quantitatively with the more accurate trend obtained with the intensities at low 2θ values. The formation of Ca_2PbO_4 ($2\theta = 17.7°$) decreases with increasing sintering time, while with Ca_2CuO_3 ($2\theta = 36.8°$) no particular trend is observed. It is generally observed that even though with increasing sintering temperature the fraction of the 2223 phase increases, the bismuth-related impurity phases also increase (Table I).

A least-squares refinement program by Garvey[48] was utilized, assuming a pseudo-tetragonal cell, to calculate the cell parameters for the 2212 and the 2223 phases (Table II). Since the composition of the sample is assumed not to change greatly, the analysis obtained should indicate true changes due to sintering time and temperature. The peaks corresponding to the 2212 phase are indexed with a tetragonal unit cell with $a = b = 5.395$ Å and $c = 30.714$ Å while the 2223 phase is also indexed with a tetragonal unit cell with $a = b = 5.431$ Å and $c = 37.081$ Å. With increasing sintering time and temperature a slight expansion of the $a = b$ axis occurs while the c axis decreases in the 2212 crystal system. In contrast, the 2223 crystal system does not show much variation for the $a = b$ axis while the c axis appears to slightly expand. This probably suggests different amounts and location of Pb substitution for Bi in the two types of superconducting phases. Variations of oxygen content with annealing temperature might also contribute in some degree to the unit cell changes of the phases in Table II. The slight lattice variation could also be due to the small Bi and Pb deficiency due to losses during preparation.

Resistance Measurement. A distribution of zero resistance temperatures (T_0) has been obtained depending upon the synthesis conditions (Figure 3). At a sintering temperature of 1133 K, a large resistance drop occurs near 100 K while the zero resistance is attained only close to 80 K. Our best sample (Pb/1143/80) displays a resistance transition onset close to 110 K and a T_0 of 98 K. Sintering at higher temperature (1153 K) shows a prominent tail indicating residual resistance. The step expected in the resistance vs temperature curve corresponding to the two distinct phases with different T_c's (80 and 110 K) is not very distinct. This could be due to a distribution of grains of high-T_c phase in the granular matrix corresponding to the lower-T_c phase. Also this suggests that the resistance arises from intergranular behavior and not from agglomerated particles of grains corresponding to isolated high-T_c and lower T_c phases.

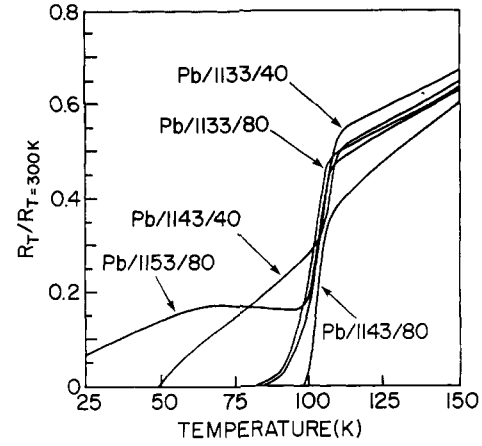

Figure 3. Resistance versus temperature profile for samples Pb/1133/40, Pb/1133/80, Pb/1143/40, Pb/1143/80, and Pb/1153/80.

Table III. Resistance at 280 K and Percent 2212 and 2223 Phases Detected by LFMA Measurements for $Bi_{1.6}Pb_{0.4}Sr_2Ca_2O_4$ Samples as a Function of Sintering Time and Temperature

sample type	resistance, mΩ/cm	% 2212 phase	% 2223 phase
Pb/1123 K/40 h	64.2	100	
Pb/1123 K/80 h	55.4	100	
Pb/1133 K/40 h	45.2	93	7
Pb/1133 K/80 h	43.2	85	15
Pb/1143 K/40 h	42.3	93	7
Pb/1143 K/80 h	40.3	73	27
Pb/1153 K/40 h	80.4	86	14
Pb/1153 K/80 h	175.2	65	35

A longer sintering time decreases the normal state resistance of the sample (Table III). This behavior might be expected due to better intergranular contact due to compaction and for samples with larger grain size, since the resistance may be dominated by grain boundary effects. Thus, an increase in grain size is expected in samples with additional sintering temperature and time. In Pb/1153/40 and Pb/1153/80 samples the nonsuperconducting impurity phases increase. Thus, these samples show a large resistance at room temperature and do not attain zero resistance when cooled below the expected transition temperature.

Scanning Electron Micrographs. A decrease in porosity and a increase in grain size is generally observed by SEM for each sample with increasing sintering time. Typical SEM micrographs for samples Pb/113/40 to Pb/1133/80 and for samples Pb/1143/40 to Pb/1143/80 are shown in Figures 4 and 5, respectively. It is observed that with both increasing sintering time and temperature there is diminution in the number of grains, indicating a

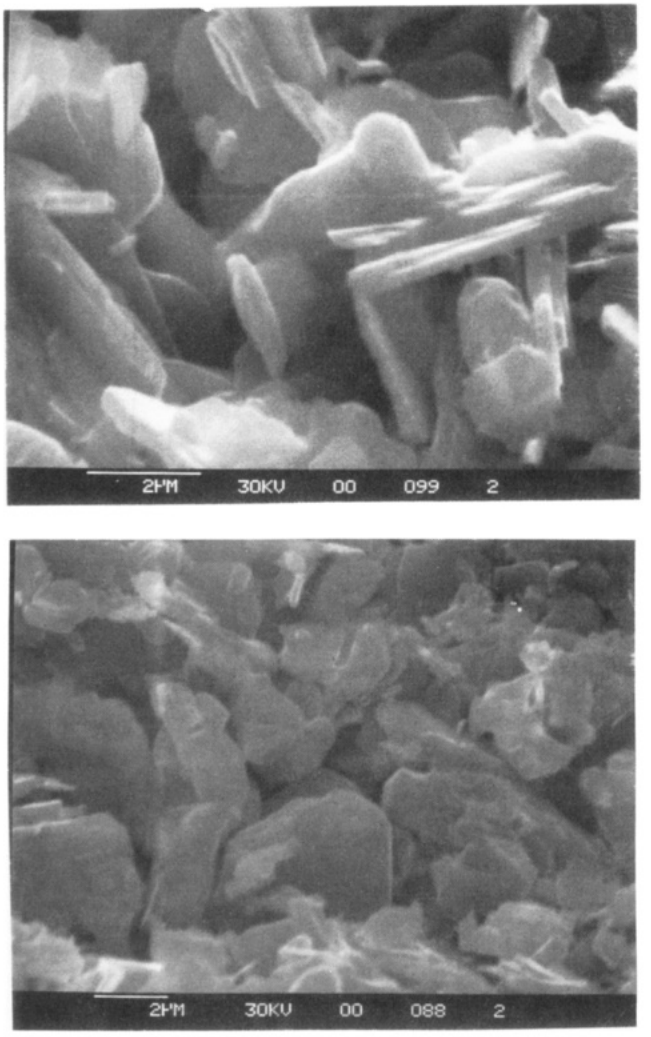

Figure 4. SEM pictures for samples Pb/1133/40 (bottom) and Pb/1133/80 (top).

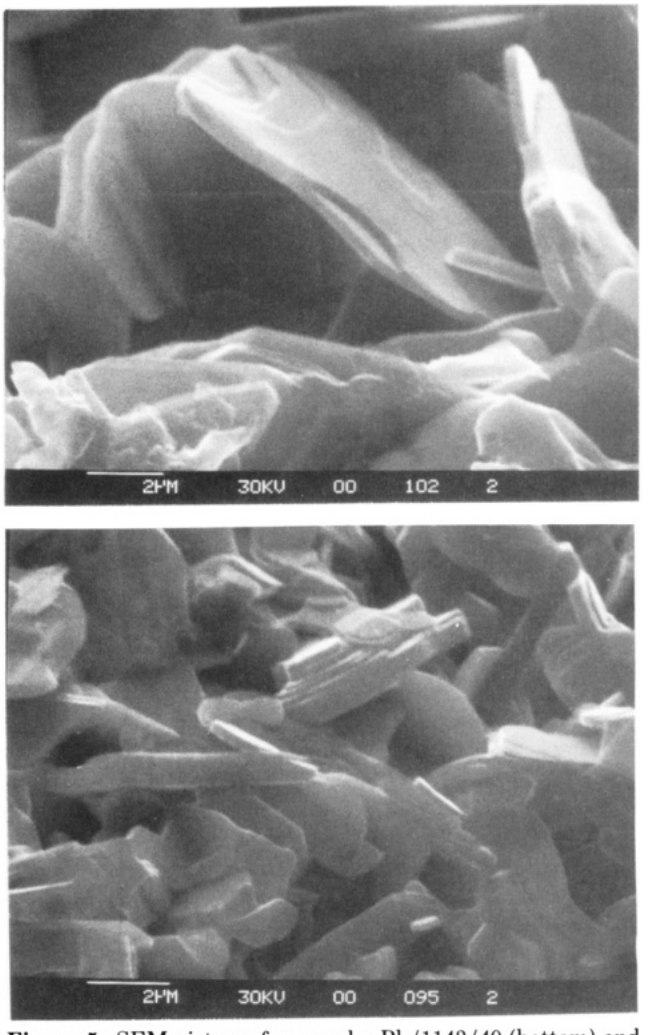

Figure 5. SEM pictures for samples Pb/1143/40 (bottom) and Pb/1143/80 (top).

decrease in the number of intergrain contacts. For samples Pb/1143/80 and Pb/1153/80 the grain size reaches nearly 10 μm and exhibits a platelike morphology as already observed for this type of ceramic.

Energy-Dispersive Absorption of X-rays. The EDAX analyses were measured on unpolished surfaces of the samples, and thus errors in the bulk composition are expected and observed on account of the dispersion of the X-ray beam from the uneven surface. However, the average composition of the bulk sample is $Bi_2Pb_{0.3}Sr_2Ca_{2.2}Cu_{2.9}$. The microanalyses confirm the formation of a multiphase system. The various compositions that could be identified correspond to the 2202, 2212, 2223, and 2220 phases.

In the Bi series of superconductive materials, the substituted amount of Pb has to be controlled in each phase. All the phases detected showed Pb substitution. On comparing the 2212 and the 2223 phases a larger (~30%) Pb substitution is observed in the 2212 phase. In the calcium- and copper-rich phases no Pb substitution was observed. This suggests that probably the Pb substitutes for Bi or Sr. However no particular structure directing trends for Pb could be observed.

The large, broad, platelike structures observed in Figures 4 and 5 correspond to the 2223 phase, while the thin, smaller slabs correspond to the 2212 phase as revealed by microprobe analyses. Some of the 2212 and 2223 phases appear to be Ca poor or both (Bi, Pb) and Sr poor. The smaller, rounded structures correspond to the 2202 phase. Thus each grain appears to be a single crystallite. Some samples showed white fluffy regions enriched in Ca and Pb with significant amounts of Sr and Bi.

Low-Field Microwave Absorption. The LFMA responses recorded for this set of lead-substituted samples are similar in shape to those obtained for the Bi–Sr–Ca–Cu–O system.[27,30-34,38] All samples were cooled in a 3-kG magnetic field from room temperature to 4 K, and the LFMA signal was recorded from −10 to 250 G through 0 G for increasing temperatures. The LFMA response as a function of temperature is similar when the sample is cooled in 0-G or 3-kG fields. A typical LFMA response as a function of temperature for Pb/1153/80 is shown in Figure 6. The maximum of the signal as a function of the external magnetic field is defined as $(d\chi''/dH)_{max}$. The peak-to-peak amplitudes, defined as the perpendicular distance between the minimum and maximum in the $(d\chi''/dH)$ versus H signal in the scan from −10 through 0 to 250 G, for the samples subjected to different sintering times and temperatures are shown in Figures 7–9.

The peak-to-peak amplitude measured in this way is useful to determine the onset transition temperature and to estimate the intensity of the LMFA response. All samples display two maxima around 40–65 and 90–115 K, suggesting the presence of two superconducting phases in these samples. A rough estimate for the relative amounts of superconducting phases formed can be evaluated from the ratio of the peak heights corresponding to the two phases from Figures 7–9 (Table III). The intensity of the

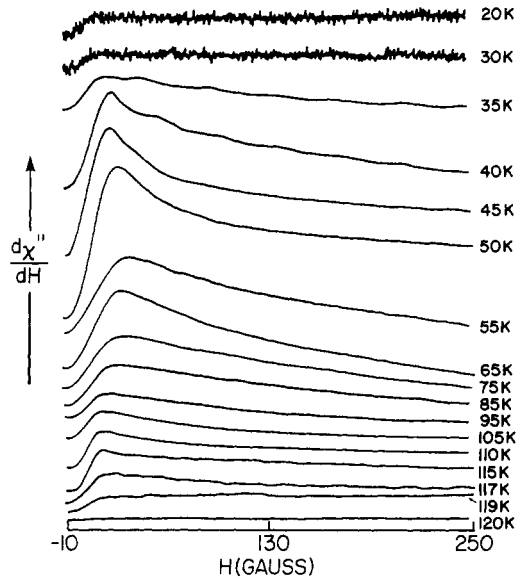

Figure 6. Example of the low-field microwave absorption of Pb/1153/80 as a function of temperature.

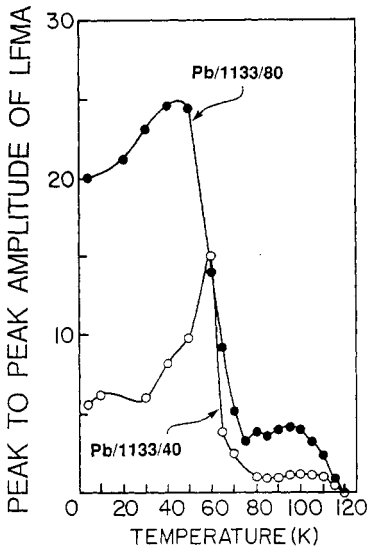

Figure 7. Intensity of the LFMA signal maximum versus temperature for samples Pb/1133/40 and Pb/1133/80.

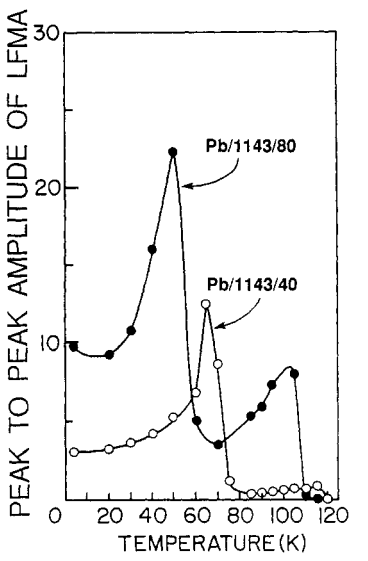

Figure 8. Intensity of the LFMA signal maximum versus temperature for samples Pb/1143/40 and Pb/1143/80.

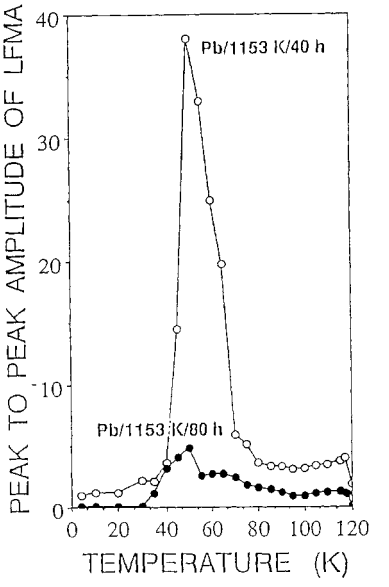

Figure 9. Intensity of the LFMA signal maximum versus temperature for samples Pb/1153/40 and Pb/1153/80.

absorption due to the low-T_c phase is 3–5 times larger than that of the high-T_c phase, which agrees with the X-ray and resistance measurements that indicate that the samples contain a greater amount of the low-T_c phase. The effect of an increasing sintering temperature for a constant sintering time is to shifts to higher temperatures the position of the two maxima in Figures 7–9. In contrast, an increase of the sintering time at a constant temperature shifts these two peaks to lower temperatures but also increases the overall intensity of the microwave absorption.

From these microwave absorption signals, it is possible to estimate the transition temperature onset of the two superconducting phases detected. The temperature onset for the high-T_c phase is generally close to 118–120 K. A transition temperature onset of 75 K for the low-T_c phase is obtained by extrapolation.

Electron Spin Resonance. No major ESR signal has been detected for this set of samples above or below the transition temperature (Figure 9). This indicates the lack of paramagnetic impurity phases.[29] The weak line around 3250 G is produced by a contaminant present in the ESR cavity. The small oscillations observed at 90 and 30 K are due to periodic temperature fluctuations in the helium flow system. The recording of the ESR signal between 130 and 6000 G reveals an unusual feature around 1000 G. At this magnetic field, the microwave absorption signal displays a minimum that appears at 90 K and also below 30 K. This particular behavior has not yet been reported for a superconducting ceramic material.

Discussion

The samples are multiphase according to XRD, LFMA, and EDAX analyses. The 2223 phase appears to increase significantly with sintering time and temperature (Table I). Several impurity phases also increase. This is likely due to the formation of the 2223 phase and a 2210 phase by disproportionation from the 2212 phase as in eq 1.

$$3Bi_2Sr_2CaCu_2O_y \rightarrow 2Bi_2Sr_2Ca_2Cu_3O_y + Bi_2Sr_2CaO_2 \quad (1)$$

However, the 2210 phase was not observed by EDAX measurements, especially in samples that show significant amounts of the 2223 phase. It could be that the byproduct $Bi_2Sr_2CaO_2$ undergoes further reaction with other phases and finally forms Bi–Sr-enriched phases such as $BiSr_3O_z$,

$Bi_{2.1}Sr_{1.8}Cu_{1.03}O_z$, and $Bi_2Sr_3Cu_2O_z$. All these impurity phases are more prominent in the samples that show larger fractions of the 2223 phase (Table I). Since all these phases are nonsuperconducting and their volume fraction increases with an increase in sintering temperature, the samples should exhibit a residual resistance as is observed for the Pb/1153/80 sample (Figure 3).

It has been shown earlier that in the Pb-free $BiSrCaCu_2O_y$ system the 2223 phase is optimized only after prolonged sintering conditions. Adding Pb to the Bi–Sr–Ca–Cu–O system increases the formation rate and the proportion of the high-T_c phase, possibly by facilitating the disproportion of the low-T_c 2212 phase as mentioned above. It has been suggested earlier that the high-T_c phase is probably formed by the reaction between the low-T_c phase and the products of decomposition of Ca_2PbO_4, which is produced during the synthesis process.[24] In the present systems the X-ray diffraction intensities corresponding to Ca_2PbO_4 decrease with increasing sintering time (Table I) and are not detected for samples showing a large fraction of the high-T_c phase. By either reaction pathway the 2223 phase could be formed. It seems that the formation of a multiphase product is an inherent property for the BiPbSrCaCuO system.

For sample Pb/1143/80 T_0 is close to 100 K, which suggests that a significant amount of high-T_c phase is present, but the LFMA results indicate that most of the microwave absorption takes place in the 40–80 K range, corresponding to the low-T_c phase. Since the recorded signal is the derivative versus magnetic field of the microwave absorption, these two maxima are at temperatures for which the LFMA changes the most rapidly as the magnetic field is scanned. These temperatures can be related to decoupling temperatures where the intergranular coupling in the bulk sample is reduced[37,57] or to critical temperatures for which flux depinning occurs.[58] For both LFMA models, the LFMA responses can be associated with characteristics of inter- and intragrain junctions.[9] This may account for differences in the broadness of the absorption peaks for samples Pb/1133/80, Pb/1143/80, and Pb/1153/40 in Figures 6–8. An increase of the sintering temperature should produce a narrower distribution of grain characteristics. For sample Pb/1153/80 the sharpess of the absorption peak is not prominent as the overall LFMA response is weak.

The difference in intensity of $(d\chi''/dH)_{max}$ between the high- and low-T_c phases for sample Pb/1143/80, for example, can be explained in terms of differential magnetic flux penetration into the sample as a function of temperature. Below 20 K, the sample is mainly in a superconducting state, and the superconducting grains are connected by direct intergrain contacts. Thus, the microwave radiation is efficiently excluded from the material. As the temperature increases, the first critical state associated with the 75 K phase is reached (i.e., first maximum in Figure 7). Above this temperature, grains of the low-T_c phase will change to a normal state while the high-T_c phase grains remain in a superconducting state. Therefore, between the two transition temperatures, the microwave radiation is able to penetrate the bulk of the sample through regions of the low-T_c phase. And the magnetic shielding properties of the material will be reduced as the temperature is increased above 75 K. This results in a greater variation of the microwave absorption from the low-T_c phase than for the high-T_c phase as the external magnetic field is increased. As the amount of high T_c phase increases with a longer sintering time (i.e., from sample Pb/1143/40 to Pb/1143/80), the intensity of the peak due to the high-T_c phase increases to 27% of the total intensity (Table III). For samples Pb/1153/40 to Pb/1153/80 the intensity of the peak due to the high-T_c phase increases to about 35% of the total intensity. In sample types Pb/1153/40 and Pb/1153/80 the X-ray results suggest that the impurity phases increase. Under such conditions, the magnetic shielding properties of the material should decrease. This should result in greater penetration of the microwaves. However, the response decreases with further sintering time as the nonsuperconducting components increase. Although the heights of the maxima cannot be directly related to the relative amounts of the two superconducting phases, the increase of the high-T_c phase contribution to the signal coincides with an augmentation of the high-T_c phase fraction measured by XRD. The trend for the volume fraction of the 2212 and 2223 phase determined by the peak heights from the LFMA results (Table III) is similar to that obtained by X-ray analysis (Table I).

Similar LFMA experiments have been reported by Calestani et al. at temperatures down to 77 K.[34] It is important to note that since the transition temperature onset measured by LFMA for the low-T_c phase in this ceramic is near 70–75 K, any estimation of the high-T_c phase component based on the absence of the low-T_c phase peak[34] is probably not valid.

The LFMA technique has been shown to be highly discriminatory and sensitive toward multiphase granular superconductors.[56] A related technique exploiting the microwave absorption response has also been used.[59–62] In this technique magnetic-field-induced changes in the microwave resistance of the sample are observed as a function of temperature. By both techniques the amplitude of the microwave response scales directly with the mass.[62,63] The volume fraction that is superconducting has been shown to be semiquantitatively comparable by LFMA and Meissner measurements.[63]

Although some characteristics of the LFMA responses have been correlated to the grain size by Dulcic et al.,[64] such a dependence is not established for the present samples because of the slow formation of superconducting phases as the grain size increases with longer sintering times. Nevertheless, it is clear from Figures 4 and 6 that as the grain size increases, the sizes of the interstices in the sample also increase. This should result in a greater penetration of the magnetic flux into the bulk sample.

In contrast to the Bi–Sr–Ca–Cu–O system for which an ESR line is usually detected above the transition temperature,[31,65,66] the lead-substituted samples do not show any significant ESR signal.[67,68] From the observations

(57) Thompson, J. R.; Brynestad, J.; Kroeger, D. M.; Kim, Y. C.; Secula, S. T.; Christen, D. K.; Specht, E. D. *Phys. Rev. B* **1989**, *39*, 6652.
(58) Nikolo, M.; Goldfarb, R. B. *Phys. Rev. B* **1988**, *37*, 6615.
(59) Kim, B. F.; Bohandy, J.; Phillips, T. E.; Adrian, F. J.; Moorjani, K. *Physica C* **1989**, *161*, 76.
(60) Moorjani, K.; Bohandy, J.; Adrian, F. J.; Kim, B. F.; Shull, R. D.; Chiang, C. K.; Swartzendruber, L. J.; Bennett, L. H. *Phys. Rev. B* **1987**, *36*, 4036.
(61) Kim, B. F.; Bohandy, J.; Phillips, T. E.; Green, W. J.; Agostinelli, E.; Adrian, F. J.; Moorjani, K.; Swartzendruber, L. J.; Shull, R. D.; Bennett, L. H.; Wallace, J. S. *Appl. Phys. Lett.* **1988**, *53*, 321.
(62) Kim, B. F.; Bohandy, J.; Moorjani, K.; Adrian F. J. *J. Appl. Phys.* **1988**, *63*, 2029.
(63) Puri, M.; Marrelli, S.; Li, L.; Cuvier, S.; Bear, J.; Kevan, L. *J. Chem. Soc., Faraday Trans.*, in press.
(64) Peric, M.; Rakvin, B.; Prester, M.; Brnicevic, N.; Dulcic, A. *Phys. Rev. B* **1988**, *37*, 522.
(65) Yuan, S. L.; Hou, B. H.; Jin, S. Z. *Mod. Phys. Lett.* **1989**, *3*, 355.
(66) Shaltiel, D.; Bill, H.; Decroux, M.; Hagemann, H.; Junod, A.; Peter, M.; Sekhar, Y. R.; Triscone, G.; Walker, E.; Yan, Y. F.; Zhao, Z. X. *Physica C* **1989**, *157*, 240.

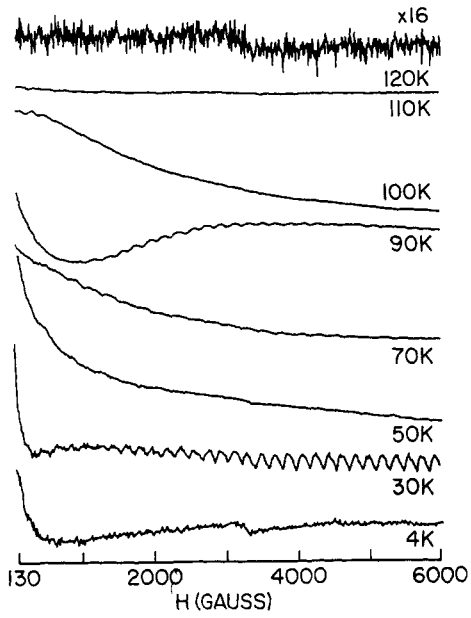

Figure 10. ESR signal between 130 and 6000 G for sample Pb/1143/80 at various temperatures.

made on sintered Bi–Sr–Ca–Cu–O samples, the paramagnetic resonance is generally attributed to Cu^{2+} species of a nonsuperconducting impurity phase.[66] Therefore, the absence of ESR for the lead-doped system implies that no major impurity phase with ESR-active Cu^{2+} ions remains after the synthesis. This does not exclude the presence of other impurities such as CuO, which is known to be ESR inactive.[66,69] Our results agree with observations made by Yuan et al.,[65] but instead of considering an increasing conversion of Cu^{2+} to Cu^{3+} species with lead addition, we suggest a structural stabilization of the superconducting phase leading to delocalization of the unpaired electron of Cu^{2+}. The particular behavior of the microwave absorption signal for magnetic fields greater than 200 G (Figure 10) remains unexplained. The negative slope of the responses at 100, 70, and 50 K may be attributed to the persistence of the microwave absorption at high magnetic fields. But the minimum at 90 K near 100 G is not presently understood.

Conclusions

The amount of high-T_c phase formation appears to be dependent on sintering time and temperature. The low-T_c phase probably undergoes a conversion process to the high-T_c phase by disproportionation. Multiphase formation seems to be an inherent property of the Bi–Pb–Sr–Ca–Cu–O system.

The low-field microwave absorption technique permits one to detect the presence of a low-T_c phase diluted in a material having a higher transition temperature, even though resistance measurements show no transition for the low T_c phase. Thus, it is important to make *both* LFMA and resistance measurements when characterizing new preparations. The relative amounts of superconducting phases formed can be compared by the LFMA technique, and similar trends are obtained by X-ray diffraction analysis. The penetration of the magnetic flux into the bulk of the sample as the temperature is raised to transition temperatures between those of high- and low-T_c phases shows an anomalous amount of microwave absorption in the low-T_c temperature region.

Acknowledgment. This material is based upon work supported by the Texas Center for Superconductivity at the University of Houston under the prime grant MDA 972-88-G-0002 from the Defense Advanced Research Projects Agency and from the State of Texas.

Registry No. $Bi_2Sr_2Ca_2Cu_3O_y$, 114901-61-0; $Bi_{1.6}Pb_{0.4}Sr_2Ca_2Cu_3O_7$, 130706-61-5; PbO_2, 1309-60-0; Ca_2PbO_4, 12013-69-3; Ca_2CuO_3, 12213-78-4; CaO_4, 12133-35-6; $SrPbO_3$, 12439-80-4; Sr_2PbO_4, 12143-42-9; $BiSr_3O_z$, 61180-93-6; $Bi_2Sr_3Cu_2O_z$, 113288-51-0.

(67) Yuan, S. L.; Jin, S. Z.; Zhu, B.; Wang, W.; Zheng, J. Q.; Zheng, G. G.; Guan, W. Y. *Modern Phys. Lett.* **1989**, *3*, 331.
(68) Jones, R.; Janes, R.; Armstrong, R.; Singh, K. K.; Edwards, P. P.; Keeble, D. J.; Harrison, M. R. *J. Chem. Soc., Faraday Trans.* **1990**, *86*, 683.
(69) Mehran, F.; Barnes, S. E.; Chandrasekhar, G. V.; McGuire, T. R.; Shafer, M. W. *Solid State Commun.* **1988**, *67*, 1187.